CrossMark

RESEARCH ARTICLE

Complex fluids affect low-Reynolds number locomotion in a kinematic-dependent manner

Francisco A. Godínez[1] · **Lyndon Koens[2]** · **Thomas D. Montenegro-Johnson[2]** ·
Roberto Zenit[3] · **Eric Lauga[2]**

Abstract In order to improve our understanding of the self-propulsion of swimming microorganisms in viscoelastic fluids, we study experimentally the locomotion of three artificial macro-scale swimmers in Newtonian and synthetic Boger fluids. Each swimmer is made of a rigid head and a tail whose dynamics leads to viscous propulsion. By considering three different kinematics of the tail (helical rigid, planar flexible, and helical flexible) in the same fluid, we demonstrate experimentally that the impact of viscoelasticity on the locomotion speed of the swimmers depends crucially on the kinematics of the tails. Specifically, rigid helical swimmers see no change in their swimming speed, swimmers with planar rod-like flexible tails always swim faster, while those with flexible ribbon-like tails undergoing helical deformation go systematically slower. Our study points to a subtle interplay between tail deformation, actuation, and viscoelastic stresses, and is relevant to the three-dimensional dynamics of flagellated cells in non-Newtonian fluids.

✉ Roberto Zenit
zenit@unam.mx

Eric Lauga
e.lauga@damtp.cam.ac.uk

[1] Instituto de Ingeniería, Universidad Nacional Autónoma de México, México, D.F. 04510, Mexico

[2] Department of Applied Mathematics and Theoretical Physics, Centre for Mathematical Sciences, Wilberforce Road, Cambridge CB3 0WA, UK

[3] Instituto de Investigaciones en Materiales, Universidad Nacional Autónoma de México, México, D.F. 04510, Mexico

1 Introduction

The fluid mechanics of swimming microorganisms has been one of the most successful areas of biophysics, and precise quantitative progress was achieved throughout the 1970s at the single-cell level (Jahn and Votta 1972; Lighthill 1975; Brennen and Winet 1977; Purcell 1977; Childress 1981). Classical work mostly focused on the relationship between the deformation kinematics of an organism and its resulting swimming speed in a Newtonian fluid. Around the same time, biologists were making considerable progress in their understanding of the different manners in which flagella, the slender cellular appendages used for locomotion, were actuated by various organisms of interests, for both bacteria and eukaryotes (Bray 2000). With the advancement of high-speed imaging techniques, microfluidic devices, and modern microscopy, the field has undergone a recent resurgence and prompted the fluid mechanics community to ask a new series of questions on some of the nonlinear aspects of locomotion (Lauga and Powers 2009; Guasto et al. 2012).
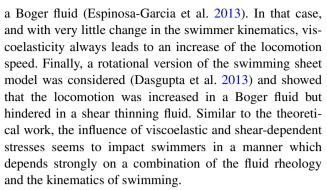
One of the currently active research questions concerns the locomotion of microorganisms in non-Newtonian fluids. Many problems relevant to biology involve the transport and locomotion in viscoelastic, shear thinning fluids, for example mucus transport by cilia in our upper lungs (Sleigh et al. 1988) or the swimming of mammalian spermatozoa in cervical mucus (Suarez and Pacey 2006). The main question under debate in this topic is whether the non-Newtonian stresses (and their possible time-complex dependence) are helping microorganisms go faster, or if instead they hinder locomotion. This is the question we attempt to answer experimentally in this paper by showing that there is no universal answer to it.

Building on early theoretical work (Ross and Corrsin 1974; Chaudhury 1979; Fulford et al. 1998), a series of asymptotic analyses considered the small-amplitude locomotion of geometrically simple waving swimmers in two (Lauga 2007b) and three dimensions (Fu et al. 2007, 2009) in viscoelastic fluids. In this limit, swimming with a prescribed stroke in a viscoelastic fluid always leads to a decrease in the swimming speed. A subsequent numerical analysis of the two-dimensional case showed that for large-amplitude motion, increase in the swimming speed was actually possible for certain waving kinematics (Teran et al. 2010). Other geometries were also considered, in particular a simplified swimmer made of three spheres (Curtis and Gaffney 2013) or a single sphere with a prescribed surface velocity (Zhu et al. 2011, 2012). Related theoretical work includes locomotion in a gel (Fu et al. 2010), in a two-phase fluid (Du et al. 2012), in a thin yield-stress film (Chan et al. 2005; Balmforth et al. 2010), in a heterogeneous porous-like medium (Leshansky 2009), and in an inelastic, generalized Newtonian fluid (Montenegro-Johnson et al. 2012; Vélez-Cordero and Lauga 2013). These theoretical results, taken together, do not show a systematic increase or decrease of the locomotion speeds of the swimmers but instead either one or the other depending on the type of swimming kinematics considered, the fluid rheology, and the physics of the coupling between the two. Note that beyond the relationship between Newtonian and non-Newtonian swimming, viscoelastic stresses can be exploited in order to devise new methods for small-scale force generation (Normand and Lauga 2008), pumping (Pak et al. 2010), swimming devices (Lauga 2009; Pak et al. 2012; Keim et al. 2012), and rheological probes (Pak et al. 2012).

Compared to the large amount of theoretical work, only a handful of experimental investigations have been devoted to the question of quantifying locomotion in complex fluids. The first study considered the model worm *Caenorhabditis elegans* in a Boger fluid displaying elasticity but with constant viscosity (Shen and Arratia 2011). The change in the fluid rheology from Newtonian to non-Newtonian did not affect the swimming kinematics of the organism and resulted in a systematic decrease in their swimming speed, in good agreement with the asymptotic investigations (Lauga 2007b). A second experiment measured the force-free motion of rotated rigid helices as a model for the locomotion of bacteria employing helical flagella (Liu et al. 2011). They showed that while small-amplitude helices were always slowed down by viscoelasticity, at a critical amplitude, a modest increase of the swimming speed was in fact possible. That observation is consistent with the two-dimensional swimming sheet results at large amplitude (Teran et al. 2010). A third experiment considered flexible swimmers actuated by an external (magnetic) field in

a Boger fluid (Espinosa-Garcia et al. 2013). In that case, and with very little change in the swimmer kinematics, viscoelasticity always leads to an increase of the locomotion speed. Finally, a rotational version of the swimming sheet model was considered (Dasgupta et al. 2013) and showed that the locomotion was increased in a Boger fluid but hindered in a shear thinning fluid. Similar to the theoretical work, the influence of viscoelastic and shear-dependent stresses seems to impact swimmers in a manner which depends strongly on a combination of the fluid rheology and the kinematics of swimming.

In this paper, we consider experimentally low-Reynolds number locomotion in two fluids: a Newtonian fluid as well as a Boger fluid with the same viscosity. We design, fabricate, and measure the locomotion velocity of three swimmers displaying qualitatively different swimming kinematics (flexible vs. rigid; two- vs. three-dimensional; constant vs. decaying actuation amplitude). We show that, with the same combination of fluids, our three swimmers show three different responses to a change from Newtonian to non-Newtonian: one displays an unchanged swimming speed, one goes systematically faster, and one slower. These experimental results allow us to conclusively demonstrate, in a controlled experimental setting and with unchanged fluids, that complex fluids affect Stokesian locomotion in a kinematic-dependent manner.

2 Experimental setup

The three synthetic swimmers we designed for our experiments have similar features and are illustrated in Fig. 1. They consist of a tail attached to a cylindrical head of circular cross section. The head is made of polypropylene in which air is trapped to achieve neutral buoyancy. Each head includes a permanent magnet (Magcraft, model NSN0658) with length and diameter of 3.18 mm possessing a remanent magnetic flux, $B_m = 1.265 \pm 0.015$ T. The permanent magnet is encapsulated and fixed in place within the cylindrical head, allowing control over the locations of the centers of gravity and flotation. In all cases, a time-varying, uniform external magnetic field is used to drive the swimmers and propulsion is achieved through the motion of the different tails.
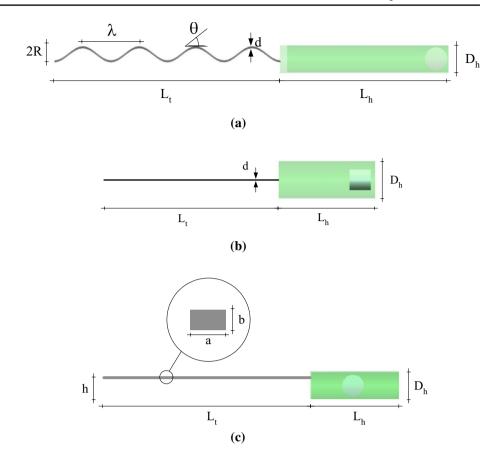
2.1 Swimmer #1: Rigid corkscrew geometry

The first synthetic swimmer is schematically shown in Fig. 1a. The permanent magnet is attached to one end of the plastic head and a rigid metallic helix is glued at the other end so that the helix axis is aligned with the head axis. The helical tail is made of steel wire with a Young's modulus $E \approx 207$ GPa, a diameter $d = 0.3$ mm, pitch angle

Fig. 1 Sketch of the three different swimmers used in this study. **a** Rigid helical; **b** flexible planar; **c** flexible helical. See text for notation and dimensions. **a** Swimmer #1. **b** Swimmer #2. **c** Swimmer #3

(a)

(b)

(c)

$\theta = 52°$, wavelength $\lambda = 7.6$ mm and tail length $L_t = 35.7$ mm. The diameter and length of the head in this case are $D_h = 4.0$ mm, and $L_h = 14.2$ mm. The external diameter of the helix is $2R = 3.5$ mm.

2.2 Swimmer #2: Rod-like flexible tail under planar actuation

A sketch of this second swimmer is shown in Fig. 1b. The permanent magnet is attached at one end of the tubular head, while a straight flexible tail is glued at the other end at the center of the cross section of the cylinder. The tail is a piece of cylindrical optic fiber of length $L_t = 25$ mm and diameter $d = 125$ μm, with a Young's modulus similar to that of glass, $E \approx 80$ GPa. The diameter and length of the head are $D_h = 5.7$ mm and $L_h = 14.7$ mm. Note that this is the swimmer used in Espinosa-Garcia et al. (2013).

2.3 Swimmer #3: Ribbon-like flexible tail under three-dimensional actuation

The third synthetic swimmer used in our study is shown in Fig. 1c. The permanent magnet is fixed in the middle of the cylindrical head and both ends of the head are sealed with silicone glue so that a pair of air bubbles is trapped to achieve neutral flotation. The tail is a flexible filament of silicon rubber with a Young's modulus $E \approx 0.025$ GPa, length $L_t = 31$ mm, and a rectangular cross section $b = 0.5$ mm in height and $a = 1$ mm in width (so it is ribbon-like). This filament is attached to one side of the head, at a distance $h = 4.0$ mm (as depicted in the figure). The diameter and length of the head are $D_h = 4.4$ mm and $L_h = 13.5$ mm.

2.4 Magnetic device for actuation

Our experimental setup consists of a Helmholtz coil pair which is mechanically coupled to a DC electric motor whose angular velocity is controlled. Each coil has a radius of 140 mm with 230 turns of 19-gauge enameled copper wire. The coil pair is fed with a DC source to generate a spatially uniform rotating magnetic field (magnitude ≈ 6 mT for a maximum current of 4 A) for a workspace of about 100 mm along the rotation axis and rotation frequencies below 10 Hz (Godinez et al. 2012). This rotating electromagnetic–mechanical device, shown schematically in Fig. 2, was used to actuate artificial swimmers #1 and #3. These swimmers were placed in a fluid-filled rectangular container (160 mm × 100 mm × 100 mm) made of transparent acrylic and located in the center of the coil system. In Fig. 3a, c, we show the field lines of the unsteady external magnetic field, $B_{HC}(t)$, and those of the
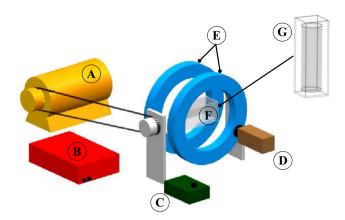
permanent magnet for the swimmers #1 and #3, respectively. The rotation axes of the swimmers are indicated with dashed lines.

In order to drive swimmer #2, the coil pair did not rotate but was kept fixed. Instead, it was energized with a DC step voltage changing sign periodically to achieve a magnetic field of alternating sign with a frequency of up to 10 Hz remaining in a single plane. This swimmer was placed inside a fluid-filled cylindrical container (diameter, $D_c = 50.8$ mm) made of transparent acrylic. As shown in Fig. 2, this container was located inside the Helmholtz coil pair which provides the driving magnetic actuation to rotate alternately (see Fig. 3b) the magnetic head, leading to planar deformation of the flexible tail and locomotion. This was the setup used in Espinosa-Garcia et al. (2013).

In all three cases, the motion of the swimmers was filmed with a digital camera and their positions and speeds were obtained by digital video image processing. We show in Fig. 4 time sequences of a swimming cycle for each of the swimmers. Swimmer #1 has a rigid tail whose shape is not modified by the external actuation or throughout the cycle; we further observe that the axis of the swimmer only displays a small amount of wobbling and essentially remains perpendicular to the plane of rotation of the magnetic field. The swimming cycle of swimmer #2, similar to that shown in Fig. 2 of Espinosa-Garcia et al. (2013), shows planar bending of the flexible tail; the time asymmetry in the tail shape leads to propulsion of the swimmer head first. Finally, the locomotion of swimmer #3 shows the three-dimensional rotation of its ribbon-like tail; as a difference with swimmer #1, the tail shape of swimmer #3 is not fixed but arises from a dynamic balance between the actuation from the rotating head, the bending and twisting of the tail, and the hydrodynamic forces. In particular, it is a function of the frequency of rotation of the magnetic field. All experiments were repeated at least fives times for each condition; the error bars in the figures below denote the standard deviation of the measurements.

In order to show that the forward motion of the three devices described above is the result of propulsive forces generated by the tails, we conducted several additional tests. We placed the head of the swimmers (without tail) in the magnetic device and found that no net motion occurred in any of the cases. For the rotating swimmers (swimmers #1 and #3), the head spun around its axis but no forward motion could be measured. For the case of the planar swimmer (swimmer#2), the head moved symmetrically from side to side, and again, no forward net motion was detected. The motion reported in this paper is thus a result of the propulsive interaction between the tail and the surrounding fluid.

Fig. 2 Electromagnetic–mechanical device used to actuate the synthetic swimmers. *A* DC motor; *B* DC source to feed coils; *C* angular speed control of the DC motor; *D* digital camera; *E* coil pair; *F* rectangular tank used to test swimmers #1 and #3; *G* cylindrical container used to test swimmer #2 (this cylindrical container was placed in a water-filled rectangular tank to avoid optical aberrations)
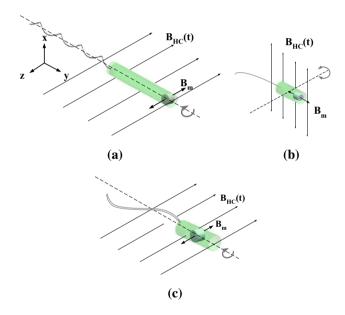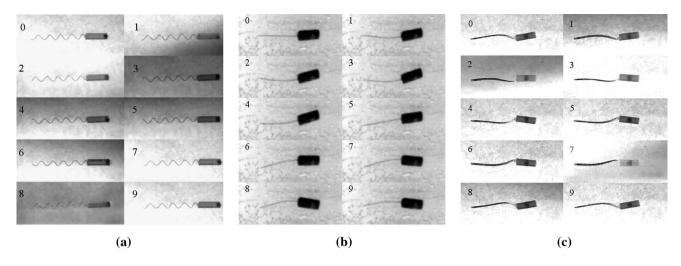

Fig. 3 Field lines of the external magnetic fields along with those of the permanent magnet in each artificial swimmer (the labels refer to the same three swimmers as in Fig. 1). In each case, the rotation axes of the swimmers are indicated by the *dashed lines*. **a** Swimmer #1. **b** Swimmer #2. **c** Swimmer #3

2.5 Fluid rheology

In our study, we use the same fluid in our experimental tests of all three synthetic swimmers. In this manner, we aim to isolate the effect of swimming kinematics. This is therefore different from the recent work of Dasgupta et al. (2013) where the kinematics were kept fixed (wave-like motion of a cylindrical surface) and instead the fluid properties were varied.

Fig. 4 Image sequence of a swimming cycle for all swimmers. In all cases, the frequency is $f \approx 3$ Hz in the Newtonian fluid; time step between each image, $\Delta t = 33.3$ ms. Note that the scales are different in each image (see text for dimensions). **a** Swimmer #1. **b** Swimmer #2. **c** Swimmer #3
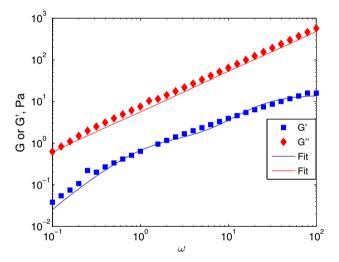
Table 1 Properties of the two fluids considered in this study: Newtonian (N) and Boger (B)

Fluid	Composition (G/W/ PaaM, %)	ρ (kg/m^3)	μ (Pa s)	n (–)	λ (s)
N	89/11/0	1390	3.5	1.0	0.0
B	84.96/15/0.04	1340	3.7	0.98	1.23

Composition: Glucose (G), water (W) or Polyacrilamide (PaaM)

Two types of fluids were prepared, a Newtonian one and viscoelastic Boger fluid. Both fluids are glucose-based water solutions. To confer elasticity to the test fluid, a small amount of polyacrylamide (Separan AP30, Dow Chemicals) is added, leading to a fluid with nearly constant viscosity and finite relaxation times (Boger 1977). In Table 1, we show the properties of the two test fluids used in our experiments (composition, density, shear viscosity, power index, relaxation time). The density, ρ, is measured using a pycnometer (Simax, 50 ml). The rheological properties were obtained using a cone-plate rheometer (TA Instruments, AT 1000N). Both steady and oscillatory tests are conducted to measure the steady shear viscosity, μ, and the storage and loss moduli, $G'(\omega)$ and $G''(\omega)$, respectively. In Fig. 5 we display the oscillatory tests conducted on the Boger fluid. The mean relaxation time is calculated considering the scheme used by Espinosa-Garcia et al. (2013), which consisted in fitting G' and G'' to a generalized Maxwell model considering 4 expansion terms. The power index for the Boger fluid, n, was very close to one, meaning that the shear viscosity is nearly independent of shear rate.

Once the Boger fluid is characterized, the Newtonian fluid is prepared by varying the amount of water in the liquid glucose to match the value of the shear viscosity of

Fig. 5 Oscillatory rheological tests conducted on the Boger fluid. The measured values G' (*filled square*) and G'' (*filled diamond*) are shown as a function of oscillating frequency ω. The *lines* show the fits to a generalized Maxwell model
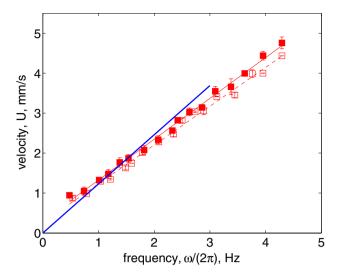
the viscoelastic fluid. Note that in all the experiments conducted in this investigation, the swimming Reynolds number, $Re = UD_h\rho/\mu$, where U is the mean swimming speed measured in the laboratory frame, is always below 6×10^{-3}, ensuring that we are always in the regime where inertial forces do not play a significant role on the locomotion of the swimmers.

3 Experimental results

In our work, we considered each of the three swimmer designs in both the Newtonian and Boger fluid for a similar

Fig. 6 Mean forward swimming speed measured in the laboratory frame, U (mm/s), as a function of the rotational frequency of the external field, $\omega/2\pi$ (Hz), of the artificial corkscrew swimmer #1: Boger fluid (*filled square*) and Newtonian fluid (*open square*). The *error bars* depict the standard error for three independent measurements. The *red lines* show a linear fit to the data. Elasticity is seen to have little impact on the swimming speed. The *thick blue line* shows the prediction from the numerical solution described in the text
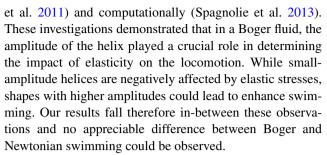
range of frequencies of the external field. As we now detail, the three swimmers lead to qualitatively different effects of viscoelasticity on the time-averaged locomotion.

3.1 Corkscrew swimmer: no impact of elasticity

In Fig. 6, we plot the swimming speed of the rigid corkscrew device (artificial swimmer #1) as a function of the rotational frequency of the magnetic field. For both fluids, we measure a swimming velocity that increases linearly with the excitation frequency. The linear dependance is to be expected in the Newtonian case, where due to the linearity of the equations of motion, the translational kinematics should scale linearly with the input frequency (Lauga and Powers 2009).

In the Boger fluid, the response should, *a priori*, be nonlinear. In very simplified terms, we can use the classic local hydrodynamic theory of locomotion by slender bodies (Lighthill 1975). If $c_\perp$ and $c_\parallel$ quantify the drag per unit length acting on the tail during motion perpendicular and parallel to its tangent, respectively, then we expect the swimming speed to scale according to $U \propto (c_\perp/c_\parallel - 1)$. Our measurements indicate that, in the range of frequencies studied, both drag coefficients are impacted by shear in a similar fashion so as to leave their ratio practically unchanged. Therefore, the swimming speed remains linear and is very similar to the Newtonian fluid.

This result is to be discussed in the light of two recent studies addressing helical locomotion experimentally (Liu

et al. 2011) and computationally (Spagnolie et al. 2013). These investigations demonstrated that in a Boger fluid, the amplitude of the helix played a crucial role in determining the impact of elasticity on the locomotion. While small-amplitude helices are negatively affected by elastic stresses, shapes with higher amplitudes could lead to enhance swimming. Our results fall therefore in-between these observations and no appreciable difference between Boger and Newtonian swimming could be observed.

In order to validate the measurements of swimming speed obtained with our setup, we numerically modeled the helical swimmer for the Newtonian case. To do so, we employ a hybrid representation of the tail and head by slender body theory and the boundary element method, respectively. The cylindrical head is modeled by a cylinder of length 10.2 mm capped at either end by spheres of radius 2 mm. A piecewise quadratic triangular mesh of this head is computed by smoothly deforming a spherical mesh generated with functions from BEMLIB (Pozrikidis 2010). The resistance matrix of this head is then calculated using routines modified from the prtcl_3d directory of BEMLIB, with constant force per unit area acting over each element. Non-singular element integrals are computed with 12-point Gaussian quadrature, while singular integrals are integrated over four flat sub-triangles in local polar coordinates with 20-point Gaussian quadrature. The tail is modeled by the helix

$$r = a(1 - \exp[-c\theta]), \quad x = r\cos\theta, \quad y = r\sin\theta,$$
$$z = b\theta, \quad \theta \in [0, \theta_m], \tag{1}$$

for $a = R - d/2 = 1.6$, $c = 2$, $b = \lambda/2\pi = 1.21$ and $\theta_m = 2\pi L_t/\lambda$ giving just over four and a half waves along the flagellum. The exponential decay in the radius as a function of theta ensures that the centre of the helical tail is attached to the centre of the swimmer. The tail is discretized into 200 straight line elements with constant force per unit length, rotating at fixed angular velocity about the helix center. The swimming speed is calculated by balancing the force the flagellum exerts on the fluid with the drag on the head, which neglects hydrodynamic interactions between the head and tail, using both Johnson slender body theory (Johnson 1980) and a line distribution of regularized stokeslets (Cortez et al. 2005; Smith 2009) of the form

$$S_{ij}^\epsilon(\mathbf{x}, \mathbf{y}) = \frac{\delta_{ij}(r^2 + 2\epsilon^2) + r_i r_j}{8\pi r_\epsilon^3} \quad \text{where} \quad r_\epsilon^2 = r^2 + \epsilon^2. \tag{2}$$

with $r_i = x_i - y_i$, $r^2 = r_1^2 + r_2^2 + r_3^2$ and $\epsilon = d/2 = 0.15$ employing 6-point Gaussian quadrature. The calculated swimming velocities between the two independent codes agree to be within 0.5 %, which is acceptable for experimental comparison. The numerically computed swimming velocity is shown as a thick blue line in Fig. 6, leading to a

good agreement particularly for small values of frequency. As the frequency increases, the slight overestimate in the swimming velocity may be attributed to an underestimate in the drag on the numerical head when compared to the experimental cylinder. Furthermore, experimentally a small amount of velocity is expected to be lost to wobbling of the swimmer axis (Man and Lauga 2013), which may explain the small of the apparent shift of the experimental data at zero frequency. Nonetheless, the results compare favorably, and validate the experimental measurements.

3.2 Planar flexible swimmer: enhanced locomotion

We now turn to the case of swimmer #2 whose flexible tail undergoes planar deformation. In Fig. 7, we plot the measured mean forward velocity for this swimmer, U (mm/s), as a function of the oscillation frequency of the planar magnetic field, $\omega/2\pi$ (Hz), for swimmer #2. These measurements are identical to those first reported in Espinosa-Garcia et al. (2013). As the oscillation frequency increases from zero, we observe that the forward velocity increases, reaches a maximum, and then decreases with ω. This dynamic behavior is expected for Newtonian fluids, as seen in classical theoretical (Wiggins and Goldstein 1998) and experimental (Dreyfus et al. 2005) studies of flexible propulsion. At small frequencies the flexible filament remains straight and induces little propulsion, while at very high frequencies, the propulsive region on the filament decreases in size, leading to a decrease of the swimming speed (Lauga 2007a). In the Boger fluid, we observe that
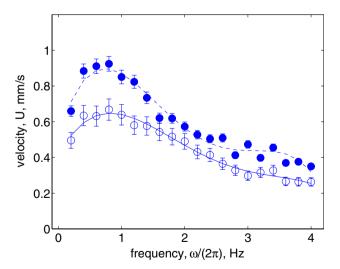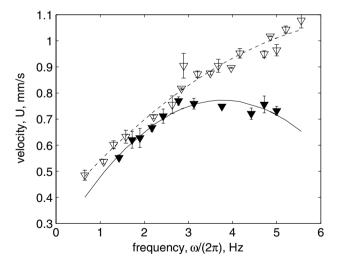
the frequency dependence of the propulsion speed is very similar to the Newtonian one, while being systematically enhanced. This enhancement is to be contrasted with the results for the rigid corkscrew swimmer (Fig. 6) where for the same range of actuation frequencies, we saw that the Boger fluid had no impact on the locomotion. As argued by Espinosa-Garcia et al. (2013), the enhancement seen in the flexible case could be due to normal stress differences acting along the tail shape. Indeed, as a difference with a rigid tail whose shape perturb the fluid in a similar fashion along its length, the deformable tail of flexible swimmer displays in general a gradient in the flapping amplitude along the tail. With normal stresses acting quadratically in the direction normal to the applied shear, it was argued by Espinosa-Garcia et al. (2013) that they could provide a net enhancement along the swimming direction.

3.3 Three-dimensional flexible swimmer: decreased locomotion

After showing results with no or positive influence of elasticity, we now turn to a case where swimming in the Boger fluid shows a systematic decrease of the locomotion speed. In Fig. 8, we plot the swimming speed developed by swimmer #3 (with a ribbon-like tail deforming in three dimensions) in the Newtonian and Boger fluids. The swimming speed in the viscoelastic fluid is systematically lower than in the Newtonian one. The trends appear to be similar up to frequencies of about 3 Hz, after which the Newtonian
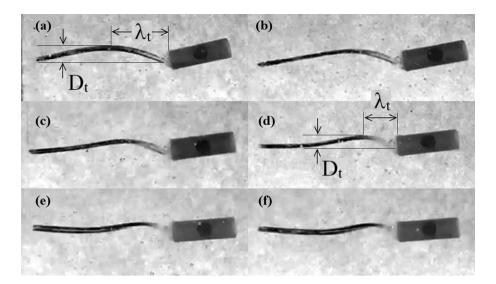

Fig. 7 Mean forward swimming speed, U (mm/s), as a function of the oscillatory frequency of the planar field, $\omega/2\pi$ (Hz), for the planar flexible swimmer (#2): Boger (*filled circle*) versus Newtonian fluid (*open circle*). The *error bars* depict the standard error for five independent measurements. The *lines* show polynomial fits to the data. Elasticity in the fluid is seen to always increase the swimming speed

Fig. 8 Mean swimming speed, U(mm/s), as a function of the rotational frequency of the three-dimensional field, $\omega/2\pi$ (Hz), for the helical flexible swimmer (#3): Boger fluid (*inverted filled triangle*) and Newtonian fluid (*inverted triangle*). The *error bars* depict the standard error for four independent measurements. The *lines* show polynomial fits to the data. Elasticity in the fluid systematically decreases the swimming speed of the device
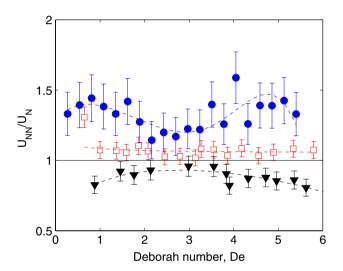
Fig. 9 Change in the shape of the three-dimensional tail of swimmer #3 with rotation frequency. This image sequence comes from tests in the Newtonian fluid. From **a**–**f** the frequency increases from 0.6 to 5.6 Hz, in 1 Hz increments

swimming speeds continue to increase with frequency, while they decrease in the Boger fluid.

In order to interpret this qualitative change in behavior, we examine the shape of the swimmer's tail as a function of frequency. This is shown in Fig. 9 in the case of a Newtonian fluid (tail shapes in the Boger fluid are similar). At low frequencies, the tail takes the shape of a half-helix with wavelength λ_t and diameter D_t (see Fig. 9a). Note that as time progresses, the shape of the swimmer is simply that illustrated in one of the panels of Fig. 9 and undergoing solid-body rotation. As ω is increased, both λ_t and D_t are observed to decrease until the critical frequency of ≈ 3 Hz (Fig. 9c). Increasing the frequency beyond no longer modifies the shape of the swimmer's tail. A more quantitative method using a superposition of the image sequences confirms this result, and beyond a critical frequency of ≈ 3 Hz, the tail takes the form of a small half-helix followed by a nearly straight filament portion, unchanged by further increases in frequency. The qualitative difference between the tail shapes below and after 3 Hz is therefore that while at low frequencies the tail generates propulsion all along its length, at higher frequencies a portion of the helix does not induce propulsion but has to be dragged along. This is responsible for the small change in slope in the Newtonian results of Fig. 8. In the Boger fluid, we conjecture that it is this qualitative change in the shape of the tail which is responsible for the decrease in the swimming speed. Without the straight portion of the shape, according to the results for rigid swimmer #1, the helical portion of the tail should keep the swimming velocity unchanged. The presence of an additional straight portion leads to increased drag with no thrust production, and a strong decrease of the swimming speed at the high Deborah numbers considered here.

Fig. 10 Ratio of non-Newtonian (U_{NN}) to Newtonian (U_N) swimming speeds, U_{NN}/U_N, as a function of the Deborah number, De for the three swimmers. Empty squares (swimmer #1, rigid corkscrew), *filled circles* (swimmer #2, planar flexible swimmer), and *filled triangles* (swimmer #3, three-dimensional flexible swimmer). The *lines* show polynomial fits to the data

4 Discussion

The main question addressed in this paper is whether elasticity in a fluid enhances or decreases the velocity of a low-Reynolds number swimmer. Past theoretical and experimental work has lead to sometimes conflicting answers. The purpose of our investigation was therefore to consider a given fluid (in this case Boger with constant viscosity and finite relaxation time), and vary the swimming kinematics. In order to compare all our results, we have gathered in Fig. 10 the results for all three swimmers with swimmer #1

in red squares, swimmer #2 in blue circles, and swimmer #3 in black triangles. Specifically, we plot the ratio between the non-Newtonian swimming speed, U_{NN}, and the Newtonian one, U_N, as function of the Deborah number, $De = \lambda\omega$. In all cases, we have added a confidence interval around the mean values for the data of $\pm$ one measured standard error. Note that in the data shown in this figure, the uncertainty is likely to be overestimated. Since ratios of two experimentally determined quantities are being shown, the estimated error bar is shown twice as much as what was determined from the standard error of the measurements. This is in accordance with standard experimental error calculation (Holman 1994).

Despite the experimental uncertainty, these results show conclusively that elasticity in the fluid affects locomotion in a manner which is strongly dependent on the kinematics of actuation on the fluid. Propulsion using a rigid corkscrew mechanism shows $U_{NN}/U_N \approx 1$, planar flapping of rod-like tails leads to $U_{NN}/U_N > 1$, while helical flapping of ribbon-like tails has $U_{NN}/U_N < 1$.

It is important to briefly discuss the possible changes in shape of the tail of each swimmer resulting form changing the fluid from Newtonian to viscoelastic. For swimmer #1, there is no change in the shape of the tail because the it is rigid; therefore, in this case, the kinematics are identical. For the flexible planar swimmer, #2, the shape of the tail does change but not significantly, as discussed by Espinosa-Garcia et al. (2013) in Fig. 8 of their paper. For swimmer #3, the changes in the tail shape resulting from the fluid are similar to those of swimmer #2. Therefore, for the three swimmers studied here, the kinematics of the tail are essentially unaffected by the nature of the fluid. Note, however, that in our study, we tested fluids that all had identical shear viscosities. For shear thinning fluids, the shape of flexible tails may in fact be strongly affected.

Based on the results presented in this investigation, it is not possible to give a general answer about the impact of viscoelasticity on the swimming performance at small Re. Each swimming protocol, i.e., each kinematic strategy, needs to be evaluated in a case-by-case manner. With this in mind, we plan to extend this investigation into two directions. We first note that in the present study, the fluid viscosity is not a function of the shear rate (Boger fluid). In most polymeric and biological fluids, both elastic stresses and shear-dependent viscosity would occur simultaneously. While we attempted here to isolate and address solely the role of elasticity, future work should address the role of shear-dependent rheology on locomotion. We further note that we have considered here and compared three qualitatively different swimming strategies, and future work should focus on a given strategy (for example helical swimming) and investigate how its geometrical details (amplitude, wavelength, etc.) affect non-Newtonian locomotion.

It is finally important to point out that in this study, we have not addressed the efficiency of swimming since we do not have access to measurements of fluid dissipation around the swimming devices. As there is, a priori, no correlation between changes in swimming speed and efficiency (Zhu et al. 2011), it would be interesting to have access to these energetics measurements. In the transitional and inertial regimes, past studies clearly show that higher swimming speeds do not always lead to higher efficiencies (Borazjani and Sotiropoulos 2009, 2010), and it would be interesting to know whether the same conclusion holds in viscous dominated flows.

References

Balmforth NJ, Coombs D, Pachmann S (2010) Microelastohydrodynamics of swimming organisms near solid boundaries in complex fluids. Q J Mech Appl Math 63:267–294

Boger DV (1977) A highly elastic constant-viscosity fluid. J NonNewt Fluid Mech 3:87–91

Borazjani I, Sotiropoulos F (2009) Numerical investigation of the hydrodynamics of anguilliform swimming in the transitional and inertial flow regimes. J Exp Biol 212:576–592

Borazjani I, Sotiropoulos F (2010) On the role of form and kinematics on the hydrodynamics of body/caudal fin swimming. J Exp Biol 213:89–107

Bray D (2000) Cell movements. Garland Publishing, New York

Brennen C, Winet H (1977) Fluid mechanics of propulsion by cilia and flagella. Ann Rev Fluid Mech 9:339–398

Chan B, Balmforth NJ, Hosoi AE (2005) Building a better snail: lubrication and adhesive locomotion. Phys Fluids 17(113):101

Chaudhury TK (1979) Swimming in a viscoelastic liquid. J Fluid Mech 95:189–197

Childress S (1981) Mechanics of swimming and flying. Cambridge University Press, Cambridge

Cortez R, Fauci L, Medovikov A (2005) The method of regularized Stokeslets in three dimensions: analysis, validation, and application to helical swimming. Phys Fluids 17(3):031,504

Curtis MP, Gaffney EA (2013) Three-sphere swimmer in a nonlinear viscoelastic medium. Phys Rev E 87(043):006

Dasgupta M, Liu B, Fu HC, Berhanu M, Breuer KS, Powers TR, Kudrolli A (2013) Speed of a swimming sheet in newtonian and viscoelastic fluids. Phys Rev E 87(013):015

Dreyfus R, Baudry J, Roper ML, Fermigier M, Stone HA, Bibette J (2005) Microscopic artificial swimmers. Nature 437:862–865

Du J, Keener JP, Guy RD, Fogelson AL (2012) Low-Reynolds-number swimming in viscous two-phase fluids. Phys Rev E 85(036):304

Espinosa-Garcia J, Lauga E, Zenit R (2013) Fluid elasticity increases the locomotion of flexible swimmers. Phys Fluids 25(031):701

Fu HC, Powers TR, Wolgemuth HC (2007) Theory of swimming filaments in viscoelastic media. Phys Rev Lett 99:258101–258105

Fu HC, Wolgemuth CW, Powers TR (2009) Swimming speeds of filaments in nonlinearly viscoelastic fluids. Phys Fluids 21(033):102

Fu HC, Shenoy VB, Powers TR (2010) Low-Reynolds-number swimming in gels. Europhys Lett 91(24):002

Fulford GR, Katz DF, Powell RL (1998) Swimming of spermatozoa in a linear viscoelastic fluid. Biorheol 35:295–309

Godinez F, Chavez O, Zenit R (2012) Design of a novel rotating magnetic field device. Rev Sci Inst 83(066):109

Guasto JS, Rusconi R, Stocker R (2012) Fluid mechanics of planktonic microorganisms. Annu Rev Fluid Mech 44

Holman J (1994) Experimental methods for engineers. McGraw-Hill, New York

Jahn TL, Votta JJ (1972) Locomotion of protozoa. Ann Rev Fluid Mech 4:93–116

Johnson RE (1980) An improved slender-body theory for stokes flow. J Fluid Mech 99(02):411–431

Keim NC, Garcia M, Arratia PE (2012) Fluid elasticity can enable propulsion at low Reynolds number. Phys Fluids 24(081):703

Lauga E (2007a) Floppy swimming: viscous locomotion of actuated elastica. Phys Rev E 75(041):916

Lauga E (2007b) Propulsion in a viscoelastic fluid. Phys Fluids 19(083):104

Lauga E (2009) Life at high Deborah number. Europhys Lett 86(64):001

Lauga E, Powers T (2009) The hydrodynamics of swimming microorganisms. Rep Prog Phys 72(096):601

Leshansky AM (2009) Enhanced low-Reynolds-number propulsion in heterogeneous viscous environments. Phys Rev E 80(051):911

Lighthill J (1975) Mathematical biofluiddynamics. SIAM, Philadelphia

Liu B, Powers TR, Breuer KS (2011) Force-free swimming of a model helical flagellum in viscoelastic fluids. Proc Natl Acad Sci USA 108:19516–19520

Man Y, Lauga E (2013) The wobbling-to-swimming transition of rotated helices. Phys Fluids 25(071):904

Montenegro-Johnson TD, Smith AA, Smith DJ, Loghin D, Blake JR (2012) Modelling the fluid mechanics of cilia and flagella in reproduction and development. Eur Phys J E 35:1–17

Normand T, Lauga E (2008) Flapping motion and force generation in a viscoelastic fluid. Phys Rev E 78(061):907

Pak OS, Normand T, Lauga E (2010) Pumping by flapping in a viscoelastic fluid. Phys Rev E 81(036):312

Pak OS, Zhu L, Brandt L, Lauga E (2012) Micropropulsion and microrheology in complex fluids via symmetry breaking. Phys Fluids 24(103):102

Pozrikidis C (2010) A practical guide to boundary element methods with the software library BEMLIB. CRC Press, Boca Raton

Purcell EM (1977) Life at low Reynolds number. Am J Phys 45:3–11

Ross SM, Corrsin S (1974) Results of an analytical model of mucociliary pumping. J Appl Physiol 37:333–340

Shen XN, Arratia PE (2011) Undulatory swimming in viscoelastic fluids. Phys Rev Lett 106(208):101

Sleigh MA, Blake JR, Liron N (1988) The propulsion of mucus by cilia. Am Rev Resp Dis 137:726–741

Smith DJ (2009) A boundary element regularized Stokeslet method applied to cilia-and flagella-driven flow. Proc R Soc Lond A 465(2112):3605–3626

Spagnolie SE, Liu B, Powers TR (2013) Locomotion of helical bodies in viscoelastic fluids: enhanced swimming at large helical amplitudes. Phys Rev Lett 111(068):101

Suarez SS, Pacey AA (2006) Sperm transport in the female reproductive tract. Hum Reprod Update 12:23–37

Teran J, Fauci L, Shelley M (2010) Viscoelastic fluid response can increase the speed and efficiency of a free swimmer. Phys Rev Lett 104(038):101

Vélez-Cordero JR, Lauga E (2013) Waving transport and propulsion in a generalized newtonian fluid. J Non-Newt Fluid Mech 199:37–50

Wiggins CH, Goldstein RE (1998) Flexive and propulsive dynamics of elastica at low Reynolds number. Phys Rev Lett 80:3879–3882

Zhu L, Do-Quang M, Lauga E, Brandt L (2011) Locomotion by tangential deformation in a polymeric fluid. Phys Rev E 83(011):901

Zhu L, Lauga E, Brandt L (2012) Self-propulsion in viscoelastic fluids: pushers vs. pullers. Phys Fluids 24(051):902